Domain structure and energy losses up to 10 kHz in grain-oriented Fe-Si sheets

Domain structure and energy losses up to 10 kHz in grain-oriented Fe-Si sheets

Cite as: AIP Advances **11**, 015220 (2021); https://doi.org/10.1063/9.0000184
Submitted: 19 October 2020 . Accepted: 20 November 2020 . Published Online: 08 January 2021

A. Magni, A. Sola, O. de la Barrière, E. Ferrara, L. Martino, C. Ragusa, C. Appino, and F. Fiorillo

Domain structure and energy losses up to 10 kHz in grain-oriented Fe-Si sheets

Cite as: AIP Advances 11, 015220 (2021); doi: 10.1063/9.0000184
Presented: 4 November 2020 • Submitted: 19 October 2020 •
Accepted: 20 November 2020 • Published Online: 8 January 2021

A. Magni,[1] A. Sola,[1] O. de la Barrière,[2] E. Ferrara,[1] L. Martino,[1] C. Ragusa,[3,a)] C. Appino,[1] and F. Fiorillo[1]

AFFILIATIONS

[1]Advanced Materials Metrology and Life Science Division, INRIM, 10135 Torino, Italy
[2]Laboratory of SATIE, 91190 Gif-sur-Yvette, France
[3]Department of Energy, Politecnico di Torino, 10129 Torino, Italy

Note: This paper was presented at the 65th Annual Conference on Magnetism and Magnetic Materials.
[a)]**Author to whom correspondence should be addressed:** carlo.ragusa@polito.it

ABSTRACT

We investigate in theory and experiment the frequency dependence of magnetic losses in Grain-Oriented 0.29 mm thick high-permeability steel sheets up to 10 kHz. Such an unusually broad frequency range, while responding to increasing trends towards high-frequency regimes in applications, is conducive to a complex evolution of the magnetization process, as imposed by increasing frequencies to a non-linear high-permeability saturable material. We show that the concept of loss decomposition, supported by observations of the domain wall dynamics through Kerr experiments, is effective in the assessment of the broadband frequency dependence of the energy loss. By calculating, in particular, the instantaneous and time averaged macroscopic induction profiles across the sheet thickness through the Maxwell's diffusion equation, the classical loss component W_{class}, versus frequency f and peak polarization J_p, is obtained. A simplified theoretical approach is pursued in this case by identifying the normal magnetization curve with the magnetic constitutive equation of the material. While the hysteresis loss W_{hyst} is shown to invariably increase with frequency, the excess loss W_{exc}, the quantity directly associated with the eddy currents circulating around the moving domain walls, tends to vanish upon increasing both frequency and induction values. The Kerr experiments actually show that, while the oscillating 180° domain walls can adjust to the depth of the induction profile by bowing at low J_p values, the magnetization reversal at high inductions and high frequencies occurs by inward motion of symmetric fronts originating at the sheet surface, according to a classical framework.

I. INTRODUCTION

Recent trends in electrical energy generation and transmission are guided by the growing role of heterogeneous and distributed renewable sources. New technologies, associated with the concept of "smart grids," are therefore developed, in order to flexibly accommodate the supply and conversion of energy.[1,2] Under these circumstances, the traditional applications of the 50 – 60 Hz power transformers combine with the operation of newly introduced devices, like the solid state transformers, where high frequencies and electronic controls, introducing substantial harmonic contents, provide a novel operative landscape. Consequently, the conventional paradigms underlying the investigation and development of the grain-oriented (GO) Fe-Si alloys need to evolve and widen their range of application.[3] Transformers employed in power electronics operate, for example, at kHz frequencies, with high order harmonics generated by Pulse Width Modulation (PWM).[4] In rotating electrical machines, GO sheets can provide an interesting alternative to the conventional non-oriented (NO) Fe-Si alloys.[5] It is shown in fact that very high speed motors display better efficiency and higher working inductions when the stator core is built by suitable combination of GO and NO sheets.[6] However, the whole matter of high-frequency response of GO alloys and its quantitative interpretation have not been assessed so far. The prevalent attitude to this problem is one of resorting to empirical/phenomenological models and formulations, like the Steinmetz's equation.[7–9] The phenomenology of energy losses at high frequencies has actually been brought to physical treatment in NO sheets, taking advantage of the fine scale of the domain structure. The Maxwell's diffusion equation has been solved in this case by a Finite Element Method (FEM), with the magnetic

constitutive law derived from a dynamic hysteresis model.[10–12] It is a complex approach, where one applies the statistics of the moving domain walls (dw) at the scale of the single finite element, which is small compared to the sheet thickness. This procedure is difficult to justify in the case of GO sheets and their broad domain structure.[13] It was suggested that, where high peak polarization values are involved in GO Fe-Si (near-rectangular loop), a step-like (saturating) magnetic constitutive law coupled to the Maxwell's diffusion equation, to be solved numerically[14] or analytically,[15] applies at all frequencies. The envisaged magnetization process consists at any frequency of symmetric reversal fronts, propagating inwards from the sheet opposite surfaces.[16] The Kerr observations show, however, that this does not happen at power frequencies, where the longitudinal bar-like domain structure always survives, whatever the peak polarization values.

In this paper, we discuss the broadband (DC ≤ f ≤ 10 kHz) frequency dependence of the energy loss measured in 0.29 mm thick high-permeability GO sheets subjected to sinusoidal polarization of peak values J_p ranging between 100 mT and 1.70 T. We first calculate the macroscopic response of the material in terms of induction profiles across the sheet thickness and classical loss $W_{class}(f)$, using the electromagnetic diffusion equation and its solution. The calculation is performed by means of a simple numerical model, lumping in the normal magnetization curve the constitutive equation of the material. This permits us to separately determine the frequency dependent hysteresis $W_{hyst}(f)$ and excess $W_{exc}(f)$ loss components and their evolution under increasing skin effect. Such evolution is measured against the direct findings on the dw dynamics provided by stroboscopic Kerr observations. These consistently show how the dw bowing, accommodating for the non-homogeneous induction profile at low inductions, makes way for symmetrical reversal fronts, propagating from the sheet surface towards mid-plane, at high inductions and high frequencies.

II. A CLASSICAL MODEL FOR THE SKIN EFFECT AND LOSSES

A. The induction profile

The eddy currents circulating in a lamination under steady dynamic excitation are assumed to form a macroscopic pattern, investing the whole cross-sectional area, and localized patterns, surrounding the moving dws. The macroscopic currents are the result of the diffusion and superposition of the localized eddies and concentrate towards the sheet surface. The ensuing counterfield, combining with the uniform applied field, does impose, at any instant of time, a definite macroscopic profile $J(x)$ to the magnetization across the sheet thickness, with obvious fluctuations at the scale of the domains. These will rearrange and adjust to such a profile by motion and bending of the dws. While the evolution of $J(x)$ versus time, responsible for the homogeneous response of the material, is associated with $W_{class}(f)$, the superimposed fluctuations, with their currents localized at the scale of the dws, give rise to the extra dynamic contribution $W_{exc}(f)$. Let us then express the relationship between macroscopic magnetic induction $b(x, t)$ and magnetic field $h(x, t)$ at any frequency and peak induction value as a function of the spatial coordinate x across the sheet thickness d ($-d/2 \le x \le d/2$) according to the classical treatment, based on the Maxwell's diffusion equation

$$\frac{\partial^2 h}{\partial x^2} - \sigma \frac{\partial b}{\partial t} = 0, \tag{1}$$

with the boundary conditions at mid-plane and surface

$$\left.\frac{\partial h}{\partial x}\right|_{x=0} = 0, \quad \left.\frac{\partial h}{\partial x}\right|_{x=\pm d/2} = \sigma \frac{\mathrm{d}}{2} \frac{\mathrm{d}B}{\mathrm{d}t} \tag{2}$$

where σ is the conductivity and $B(t)$ is the instantaneous induction of peak value B_p averaged over the sheet thickness.

The actual constitutive relation $b(h)$ is hysteretic in nature and its use in (1) would require a cumbersome numerical procedure.[10,11] To simplify the matter, we identify here the magnetic constitutive law with the normal magnetization curve. Equation (1) is then solved by standard finite elements calculations, using the fixed point method.[10,11] The sheet thickness is subdivided in 100 layers and the macroscopic profile $J(x, t)$ of the polarization is calculated at any instant of time, for any measured J_p value, at the measuring frequencies. Fig. 1 provides an example of the classically predicted behavior of the local peak polarization $J_p(x)$ across the sheet thickness at low inductions (average J_p = 0.25 T). Lack of flux penetration can be appreciated in this case on increasing the frequency beyond about 200 Hz. The sheet interior soon attains a state of near-zero magnetization upon further frequency increase and at 10 kHz the magnetization change is predicted to occur within a ~50 μm thick surface layer. With higher (thickness averaged) J_p values, however, the magnetization tends to approach the saturated state at the surface and the predicted $J_p(x)$ profile takes a sharper behavior (see inset in Fig. 1). At f = 10 kHz and J_p = 1.0 T, a neat separation is

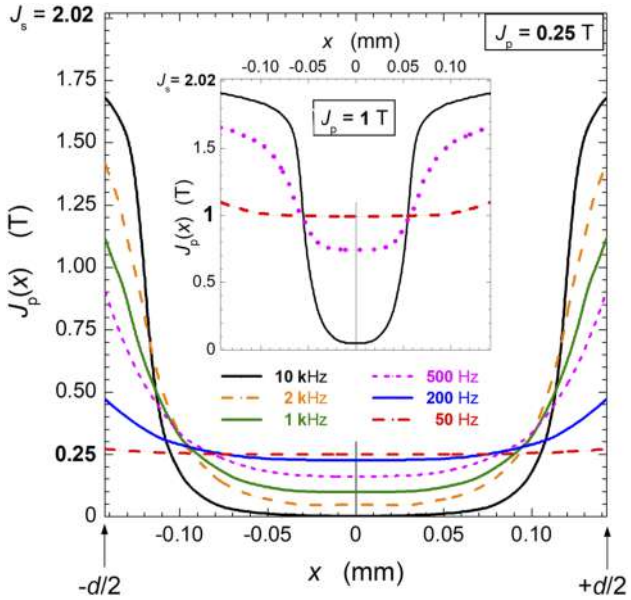

FIG. 1. Profiles of the classically calculated peak polarization value $J_p(x)$ across the 0.29 mm thick GO sheet and their dependence on the magnetizing frequency for average peak polarization J_p = 0.25 T. The inset shows the evolution taken by such profiles for J_p = 1.0 T.

then observed to occur across the sheet thickness between an outer active region and an inner dead core. At very high inductions we eventually fall in the classical problem of magnetization reversal in a highly nonlinear material.[14–17] Fig. 2, concerning the classical eddy current calculation at f = 10 kHz and J_p = 1.7 T, shows how reversal fronts are created and predicted to symmetrically proceed, at any instant of time, from the opposite sheet surfaces towards the sheet mid-plane along any semi-cycle. It is also shown that the $J_p(x)$ profile suffers in this case only a minor depression at x = 0, as imposed by the need to reach a high J_p value. The front wave phenomenon appears then to be a specifically high-frequency effect, at odds with a similar effect postulated to occur in highly homogeneous materials (e.g., fine-grained non-oriented alloys) also at low frequencies.[14,15] Kerr observations at power frequencies show that, even when cycled between $\pm J_p$ values not far from saturation (e.g., J_p/J_s = 0.91), a GO sheet exhibits the typical mechanisms of nucleation and growth of longitudinal domains by 180° dw motion.[18] The question appears then one of understanding the role of the dws across a broad range of frequencies and the way the magnetization process can eventually end into a near-classical behavior. This is directly related to the phenomenology of magnetic losses and its assessment. It is in any case immediate to obtain in all cases, via the solution of (1) and use of the Poynting theorem, or, equivalently, the integration of the square of the current density across the sheet thickness, the classical loss component $W_{class}(J_p, f)$.

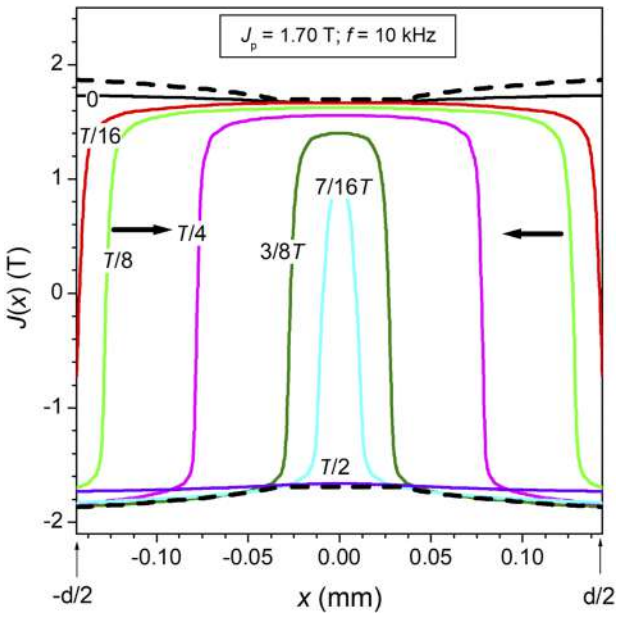

FIG. 2. Reversal fronts symmetrically proceeding inwards from the opposite sheet surfaces at high frequencies and high induction values, as predicted to occur by the classical approach in the 0.29 mm GO sheet. The calculations are made using a constitutive equation coincident with the normal magnetization curve. The fronts are shown at different instants of time (T = 1/f) along a semi-cycle taken at 10 kHz between J_p = ±1.7 T. The dashed lines show the corresponding cross-sectional profiles of the peak polarization values $\pm J_p(x)$.

III. EXPERIMENTAL METHOD

A 0.29 mm thick high-permeability Fe-Si GO alloy (M2H type) was subjected to static and dynamic characterization up to 10 kHz. The measurements were performed under controlled sinusoidal induction waveform by means of a broadband calibrated digital hysteresisgraph-wattmeter. Two different magnetizer configurations were adopted. First, an appropriate number of 300 mm × 30 mm strips, cut along the rolling direction, were tested by conventional Epstein frames, according to the standards IEC 60404-2 and IEC 60404-10. By this method, the lowest J_p values (100 mT and 250 mT) could be covered till 10 kHz. In order to deal with manageable signals, the upper J_p-f corner was investigated by means of a single-strip tester, where the GO strip, surrounded by a single-layer magnetizing solenoid, is inserted between the pole faces of a laminated double-C yoke. A few-turn secondary coil is tightly wound at the strip centre and an H-coil is placed on top of it. The turns of the windings are all properly spaced, in order to avoid capacitive effects in the kilohertz range, and single-shot measurements guarantee negligible sample heating. A detailed description of this setup is provided in Ref. 19. A sufficiently wide overlapping $J_p - f$ region could be covered with both Epstein frame and single-strip H-coil method, within ±2% agreement between the respective loss figures. The full DC normal magnetization curve was measured by means of ballistic setup, according to the point-by-point method.[20]

Dynamic Kerr observations were carried out by stroboscopic imaging. The magneto-optical setup employs an X-Cite series 120 lamp whose light is filtered, polarized and detected by a gated intensified charge-coupled device (CCD) camera (Picostar LaVision). This permits one to acquire equally time-spaced images at given frequency along the magnetization loop. The acquisition is triggered by a signal with an adjustable phase with respect to the signal that drives the magnetization of the sample. The signals are controlled by an Agilent 33522A function generator and visualized by means of a LeCroy 816Zi oscilloscope. The magnetization of the sample, which is subjected to a tensile stress of 9 MPa, is guaranteed by a split solenoid powered by a NF HSA4052 (DC - 500kHz) power amplifier. With this relatively small tensile stress, exclusively applied on the magneto-optically tested strips, shrinking and partial disappearance of the flux-closing supplementary lancet domain structure occur. This improves clarity and repeatability of the stroboscopically collected individual magneto-optical images, with minor effects on the macroscopic magnetic behavior of the high-permeability GO sheet. This move is justified by the qualitative character of the information retrieved by the Kerr imaging. The sample induction is detected by means of a 3-turn pickup coil, wound close to the investigated specularly polished and ZnS area. Each magneto-optical image (resolution 0.5 μm/pix), detected on a 5 mm diameter spot, is the average of 9000 frames, from which the usual background subtraction is made. The sample temperature, monitored by a Pt100 resistance thermometer, was allowed to rise during acquisition by a maximum of 20 °C.

IV. MAGNETIC LOSSES, DOMAINS WALL DYNAMICS, AND THEIR FREQUENCY EVOLUTION

Whatever the frequency range, the domain structure, and the skin depth, the energy loss decomposition method invariably applies

to the analysis of the magnetic losses. It requires, as a first step, the calculation of the classical loss component. As the $J_p(x)$ profiles in Fig. 1 suggest, the standard analytical formula $W_{class} = \pi^2/6\sigma d^2 J_p^2 f$, requiring uniform induction across the sample cross-section, does not apply in these GO sheets above a few hundred Hz. We are therefore obliged to resort to more complex approaches, like the one discussed in Sec. II. Relying then on the abovementioned calculations, we proceed to the broadband loss decomposition, examples of which are shown in Figs. 3a and 3b. These refer to low (J_p = 0.25 T) and high (J_p = 1.70 T) induction values, respectively. It is apparent in these figures that, with the emergence of the skin effect, the paths followed by W_{hyst}, W_{class}, and W_{exc} at high frequencies are quite different at low and high inductions. In particular, W_{exc} dominates at such frequencies for J_p = 0.25 T, while a major contribution to the loss W comes from W_{class} for J_p = 1.70 T. W_{hyst} is observed, at the same time, to remarkably increase with f at the lowest induction, but it always plays a minor role beyond a few hundred Hz.

The starting point of the loss analysis is the previously discussed calculation of W_{class}, as derived, together with the $J_p(x)$ profile, from the diffusion Eq. (1). It is apparent, looking at such profiles, that the local $W_{hyst}(x)$ will increase together with $J_p(x)$ on going from the sheet core to the surface. At low frequencies, where the skin effect is not an issue, the hysteresis loss $W_h(J_p)$ is frequency independent, and can be obtained according to a straightforward extrapolation of the measured loss to zero frequency.[21] On the other hand, the present experiments show that a power law $W_{hyst} = kJ_p^\alpha$ for the dependence of W_{hyst} on J_p applies, with k = 14.15 and α = 1.85 up to J_p = 1.5 T and k = 15.6 and α = 2.95 at higher J_p values (loss units in J/m^3). By taking into account that the quasi-static loss W_{hyst} is generated by very localized dissipative dw processes (Barkhausen jumps), we can easily retrieve its contribution at any frequency and J_p value by integrating the local W_{hyst} along the $J_p(x)$ profile

$$W_{hyst}(J_p, f) = \frac{1}{d}\int_{-d/2}^{d/2} W_{hyst}(x)\mathrm{d}x = \frac{1}{d}\int_{-d/2}^{d/2} kJ_p^\alpha(x)\mathrm{d}x. \quad (3)$$

Once $W_{class}(f)$ and $W_{hyst}(f)$ are calculated, the excess loss component $W_{exc}(f) = W(f) - W_{hyst}(f) - W_{class}(f)$, where $W(f)$ is the measured energy loss, is obtained at all J_p values.

Looking at the examples shown in Fig. 3, one can see how the prediction of the statistical theory of losses, where, for given J_p, W_{hyst} is constant, $W_{class}(f)$ is, as previously recalled, a linear function of f, and $W_{exc}(f)$ is analytically formulated via defined statistical parameters,[22] does not fully apply beyond about 200 Hz, where the theoretical $W_{exc}(f)$ (STL line) deviates from the obtained $W_{exc}(f)$. It is noted that such a deviation reflects, on approaching the kHz range, an important role of the dw processes at low inductions and a decreasing one at high inductions. We find, in particular, that about 70% of the measured loss $W(f)$ is contributed by $W_{exc}(f)$ at 10 kHz and J_p = 0.25 T, while for J_p = 1.70 T, 95% of it is covered at the same frequency by $W_{class}(f)$. To note also that the curve $W_{class}(f)$ at J_p = 0.25 T versus f suffers predictable slope changes under increasing frequency, in qualitative agreement with the corresponding behavior of the permeability at the sheet surface $\mu_{r,surf}$.

supplementary material regarding the evolution of the magnetization process versus f and J_p can be gained looking directly at the dw dynamics by the stroboscopic Kerr experiments. We provide in Figs. 4 and 5 some images taken on a well-oriented (110) [001] grain at low and high inductions and different frequencies. Fig. 4 shows an example of domain structure observed along a semi-cycle taken between J_p = ± 0.50 T at 500 Hz and 10 kHz. A regular oscillatory motion of the walls, including bowing, is observed at 500 Hz. At 10 kHz, near complete disappearance of the dws at the surface takes

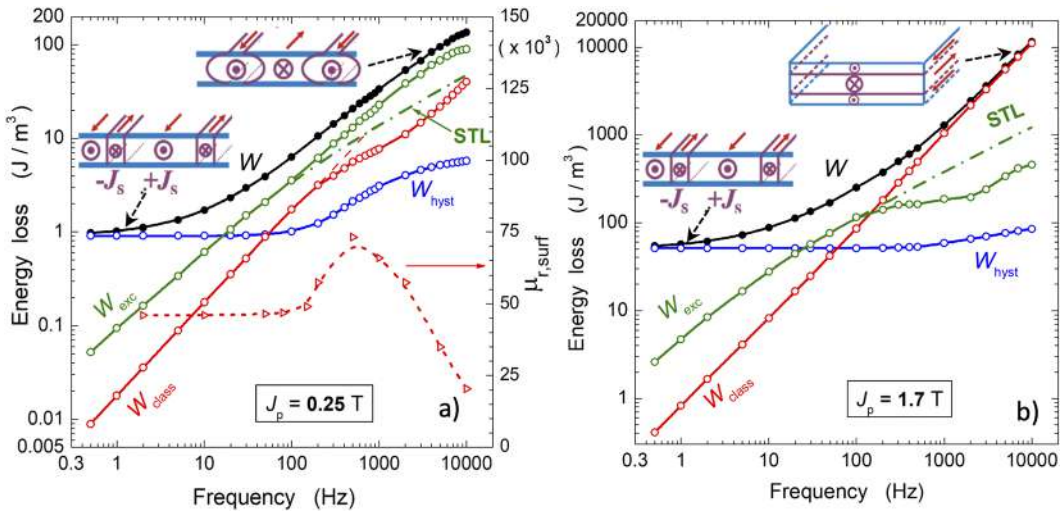

FIG. 3. DC-10 kHz loss decomposition in the 0.29 mm thick GO sheet at low and high inductions. Largely different behaviours of the loss components for J_p = 0.25 T (a) and J_p = 1.70 T (b) take place beyond a few hundred Hz, because of the emerging non-homogeneity of the induction across the sheet thickness. To note (a) the behaviour of the permeability $\mu_{r,surf}$ at the sheet surface versus f, which correlates with the behaviour of W_{class}, and the prediction of W_{exc} by the statistical theory of losses (STL line), which deviates from the experimental result upon emerging skin effect. The insets provide a qualitative scheme of the domain structure at low and high magnetizing frequencies, as envisaged by the model and induced from the dynamic Kerr observations.

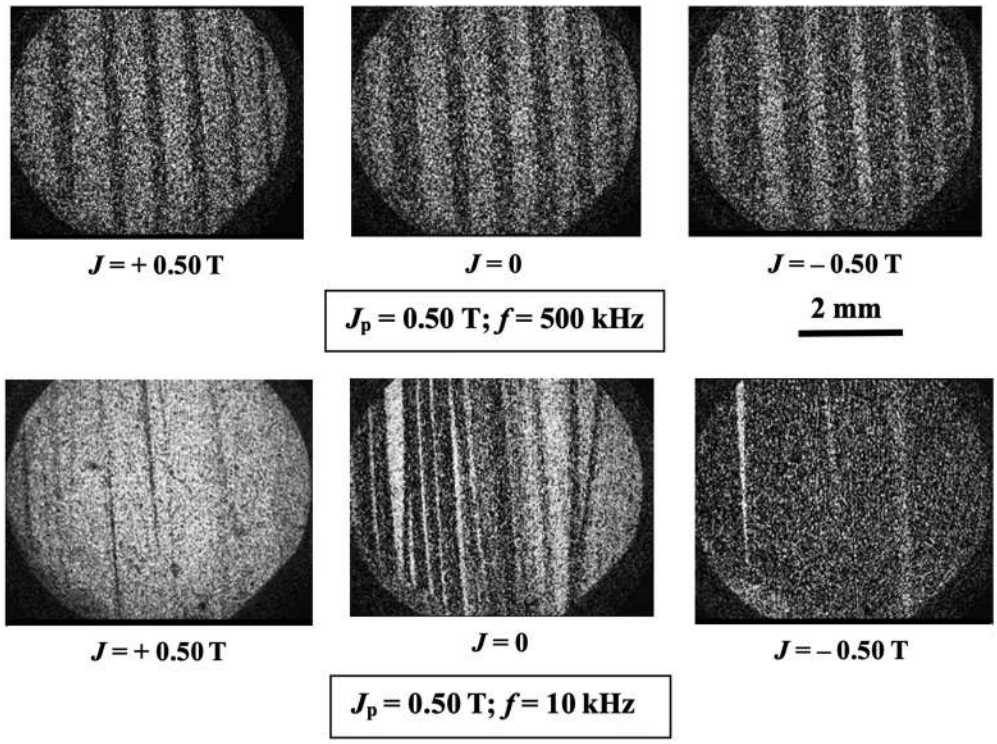

FIG. 4. Domain structure in a well oriented grain and its evolution along a semi-cycle between ± 0, 50 T at 500 Hz and 10 kHz.

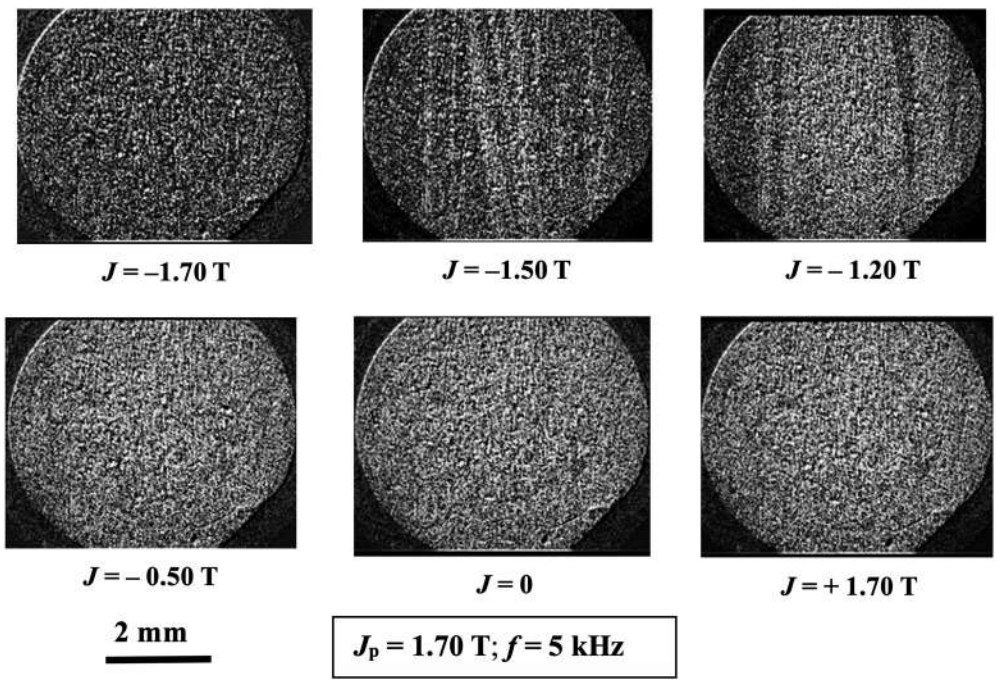

FIG. 5. As in Fig. 4 along an ascending semi-cycle run between –1.70 T to +1.70 T at 5 kHz.

place, following multiplication and strong bowing. The antiparallel 180° dw structure is, however, preserved and it reappears in full, with denser population with respect to f = 500 Hz, on the return from J_p. We conclude that at sufficiently low induction the magnetization reversal occurs at high frequencies by dw motion and bowing, consistent with the persisting large contribution of $W_{exc}(f)$ to the measured loss $W(f)$. Quite a different picture emerges in Fig. 5 from the Kerr sequence at 5 kHz taken along the semi-cycle with J_p = ±1.70 T. Starting from the fully saturated surface state observed at $J = J_p$, oppositely directed domains nucleate and grow at the surface, to eventually form a full reverse layer well before attaining the demagnetized state. This process, symmetrically occurring on the opposite sheet surface, will expectedly proceed by a mechanism close to the front reversal motion predicted by the classical model, as sketched in Fig. 2. If this is the case, little loss contribution to the measured $W(f)$ is expected to come from moving dws, as demonstrated by the faint proportion of $W_{exc}(f)$ predicted in Fig. 3b. This conclusion is further substantiated by the comparisons made between the measured and the classically predicted hysteresis loops, when obtained in the upper J_p-f corner. We see in Fig. 6 how at 10 kHz and J_p = 1.7 T the classical loop computed via Eq. (1) and the measured one have remarkably close shape and area. The slightly higher area of the experimental loop accounts for residual contribution by the dw motion, in agreement with the high-frequency loss decomposition shown in Fig. 3b. The slightly re-entrant shape of the experimental loop is related to the threshold field required, as shown in Fig. 5, to start the nucleation of the surface domains. It is finally noted its close similarity with the hysteresis loop (dashed line) calculated for an ideal step-like constitutive equation.[16]

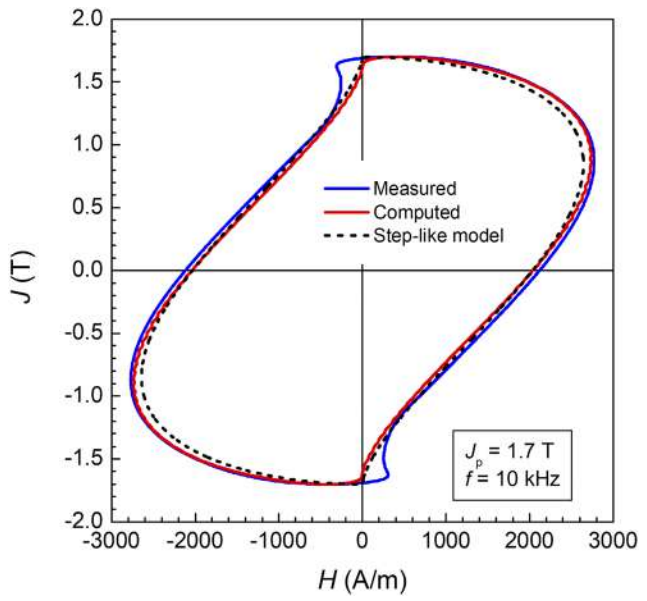

FIG. 6. The hysteresis loop classically computed via the diffusion Eq. (1) compares with the hysteresis loop measured at 10 kHz and J_p = 1.70 T, in good agreement with a magnetization mechanism occurring by the inward motion of reversal fronts, as sketched in Fig. 2. A small contribution to dissipation by dw motion results in a slightly wider experimental loop. To note a threshold mechanism at the remanence point, which descends from the nucleation of surface domains, as revealed by the images of Fig. 5. The dashed line is calculated, for the sake of qualitative comparison, in the ideal case of a step-like constitutive equation ranging between equivalent saturation values J_s = ±1.92 T.[16]

V. CONCLUSIONS

Magnetic losses have been investigated in grain-oriented high-permeability 0.29 mm thick Fe-Si sheet upon a wide range of peak polarization values (100 mT ≤ J_p ≤ 1.7 T) and frequencies (DC – 10 kHz). The loss properties have been assessed in the framework of the loss separation concept, generalized to cover the skin effect phenomena in the high-frequency region. We aim in this way at retrieving physical information on the broadband magnetization process in materials nowadays exposed to widening applicative areas, while overcoming the limitations of the empirical-phenomenological approaches proposed in the available literature. Looking for a manageable numerical treatment, the actual hysteretic magnetic constitutive equation is identified with the normal magnetization curve, which is inserted in the Maxwell's diffusion equation. This is solved by a simple finite element algorithm. The macroscopic induction profiles versus sheet thickness as a function of J_p and f and the related classical energy loss component are thereby calculated. The familiar phenomenon of propagation of magnetization reversal fronts from the sheet surface to the mid-plane occurring along a semi-cycle is, in particular, retrieved in the upper J_p-f corner. With the induction profile and the classical energy loss component W_{class} available over the whole frequency range, it is a simple matter to calculate the hysteresis W_{hyst} and the excess W_{exc} loss components, that is, to evaluate the evolution of the domain wall processes across the J_p-f matrix. Such processes are then recognized by stroboscopic Kerr observations of the frequency dependent domain structure and dw dynamics. We obtain that $W_{dw} = W_{exc} + W_{hyst}$ prevail at all frequencies over W_{class} at the lowest induction values, where the eddy currents localized at dws (either straight or bowed) are the major source of energy dissipation. The macroscopic eddy current patterns, responsible for W_{class}, dominate instead upon increasing J_p at the highest frequencies, the higher J_p the broader the frequency range where this occurs. In the limit of high peak polarizations (e.g., J_p = 1.7 T), the oscillatory motion of the 180° dws transforms, on attaining the kHz range, into a through propagation of magnetization reversal fronts. Consequently, W_{dw} becomes negligible and the classical approach is sufficient for a reasonably accurate prediction of the measured losses.

SUPPLEMENTARY MATERIAL

See the supplementary material for (1) DC magnetization curves measured in the 0.29 mm thick GO sheet by means of a ballistic setup, according to the point-by-point method; (2) a set of profiles of the classically calculated peak polarization value $J_p(x)$ across the 0.29 mm thick GO sheet and their dependence on the magnetizing frequency; (3) DC-10 kHz loss decomposition at four different peak polarization values; (4) a photograph of the stroboscopic magneto-optical setup used for dynamic domain imaging; (5) and (6) evolution along a semi-cycle of the domain structure at different frequencies and peak inductions.

DATA AVAILABILITY

The data that support the findings of this study are available from the corresponding author upon reasonable request.

REFERENCES

[1] P. Siano, Renewable Sustainable Energy Rev. **30**, 461 (2014).
[2] H. Ichou, D. Roger, M. Rossi, T. Belgrand, and R. Lemaître, J. Magn. Magn. Mater. **504**, 166658 (2020).
[3] M. A. Shamsuddin, F. Rojas, R. Cardenas, J. Pereda, M. Diaz, and R. Kennel, Energies **13**, 2319 (2020).
[4] T. Belgrand, R. Lemaître, A. Benabou, J. Blaszkowski, and C. Wang, AIP Advances **8**, 047611 (2018).
[5] G. Parent, R. Penin, J. P. Lecointe, J. F. Brudny, and T. Belgrand, IEEE Trans. Magn. **49**, 1977 (2013).
[6] L. Gao, L. Zeng, J. Yang, and R. Pei, AIP Advances **10**, 015127 (2020).
[7] K. Foster, F. E. Werner, and R. M. Del Vecchio, J. Appl. Phys. **53**, 8308 (1982).
[8] R. Liu and L. Li, IEEE Trans. Pow. Electr. **36**, 2009 (2020).
[9] J. Mühlethaler, J. Biela, J. W. Kolar, and A. Ecklebe, IEEE Trans. Pow. Electr. **27**, 953 (2012).
[10] C. Appino, G. Bertotti, D. Binesti, O. Bottauscio, M. Chiampi, J. P. Ducreux, F. Fiorillo, M. Repetto, and P. Tiberto, J. Appl. Phys. **79**, 4575 (1996).
[11] L. R. Dupre, O. Bottauscio, M. Chiampi, M. Repetto, and J. A. A. Melkebeek, IEEE Trans. Magn. **35**, 4171 (1999).
[12] C. Beatrice, C. Appino, O. de la Barrière, F. Fiorillo, and C. Ragusa, IEEE Trans. Magn. **50**, 6300504 (2014).
[13] S. E. Zirka, Y. I. Moroz, S. Steentjes, K. Hameyer, K. Chwastek, S. Zurek, and R. G. Harrison, J. Magn. Magn. Mater. **394**, 229 (2015).
[14] S. E. Zirka, Y. I. Moroz, P. Marketos, A. J. Moses, D. C. Jiles, and T. Matsuo, IEEE Trans. Magn. **44**, 2113 (2008).
[15] C. Serpico, C. Visone, I. D. Mayergoyz, V. Basso, and G. Miano, J. Appl. Phys. **87**, 6923 (2000).
[16] G. Bertotti, *Hysteresis in Magnetism* (Academic Press, San Diego, CA, 1998), p. 407.
[17] F. J. Friedlaender, Trans. AIEE, Part I **75**, 268 (1956).
[18] R. Schaefer, I. Soldatov, and S. Arai, J. Magn. Magn. Mater. **474**, 221 (2019).
[19] O. de la Barriere, C. Ragusa, M. Khan, C. Appino, F. Fiorillo, and F. Mazaleyrat, IEEE Trans. Magn. **52**, 2001204 (2016).
[20] F. Fiorillo, *Measurement and Characterization of Magnetic Materials* (Academic-Elsevier, San Diego, CA, 2004), p. 340.
[21] G. Bertotti, IEEE Trans. Magn. **24**, 621 (1988).
[22] E. Barbisio, F. Fiorillo, and C. Ragusa, IEEE Trans. Magn. **40**, 1810 (2004).